# New Technique for Efficiency Enhancement of Film Electrodes Deposited by Argon Gas Condensation from Metal Chalcogenide Sources

*Nordin Sabli[1], Zainal Abidin Talib[1,\*], Wan Mahmood Mat Yunus[1], Zulkarnain Zainal[2], Hikmat S. Hilal[3], Masatoshi Fujii[4]*

[1] Department of Physics, Faculty of Science, Universiti Putra Malaysia, 43400 UPM Serdang, Selangor, Malaysia
[2] Department of Chemistry, Faculty of Science, Universiti Putra Malaysia, 43400 UPM Serdang, Selangor, Malaysia
[3] SSERL, Department of Chemistry An-Najah N. University, PO Box 7, Nablus, West Bank, Palestine
[4] Department of Molecular Science, School of Medicine, Shimane University, Izumo, Shimane, 693-8501, Japan
[\*]E-mail: zainalat@science.upm.edu.my

This work describes a new technique to enhance photoactivity of metal chalcogenide-based semiconductor film electrodes deposited by thermal vacuum evaporation under argon gas flow. The experimental work involves controlling a number of parameters such as type of source material ($S_M$ = SnSe, $Cu_2SnSe_3$ and $Cu_2ZnSnSe_4$), substrate temperature ($T_S$ = room temperature RT, 100, 200, 300 °C), argon gas flow rates ($V_A$ = 5, 10, 15, 25 $cm^3$/min) and temperature of annealing ($T_A$= 150, 250, 350, 450 °C) under nitrogen atmosphere. The effects of varying each parameter on structural, morphological, compositional, photoresponse and optical properties of the deposited electrode were studied. The film deposited at $T_S$ = 100 °C under $V_A$ = 25 $cm^3$/min from $Cu_2ZnSnSe_4$ (CTZSe) source showed highest photoactivity (p %) value 55.7 % compared to films deposited from SnSe (TSe) and $Cu_2SnSe_3$ (CTSe) sources, with p % values of 8.3 % and 34.8 %, respectively. Thus, using the quaternary $Cu_2ZnSnSe_4$ compound as a source material, offered a new inroad to prepare photoactive thin film electrodes using the argon gas condensation (AGC) technique, simply by varying argon gas flow rate.

## 1. INTRODUCTION

Higher photoresponse and lower dark current are desired solar cell parameters [1 - 7]. Solar cells based on metal chalcogenide film electrodes are no exception. Film electrode crystallinity is one factor that affects its photoresponse. In photoelectrochemical (PEC) solar cells, the two parameters, photoresponse and lower dark current become more important as the film electrode is immersed inside the electrolyte solution. Film uniform coverage and efficient adherence to the substrate are necessary; otherwise leakage currents may occur causing higher dark currents and lower conversion efficiencies [8 - 13].

Vacuum evaporation is a suitable method to prepare film electrodes, especially in cases of metal chalcogenide materials [3, 14 - 24]. Metal chalcogenides are easy to handle in thermal vacuum evaporation as the source compound decomposes into atoms/ions which recombine again during deposition [3]. This process is different from organic material processes where the compound totally decomposes and may not yield the original structure of the organic material. The basic assumption is that by changing deposition parameters such as substrate temperature [3, 25 - 27], argon gas flow rate [28 - 29], annealing temperature [ 13, 20, 30, 31, 32 ] and source material [33, 34] from binary, ternary and quaternary systems, film electrode crystallinity and surface coverage morphology can be enhanced. Thus electrode photoactivity or photoresponse can be enhanced by controlling deposition parameters.

Researchers reported the deposition of binary metal chalcogenides such as SnSe [14, 35] and ZnSe [15] under AGC method, but with no reference to their electrochemical properties. PEC characteristics of ternary and quaternary compounds, such as CTSe and CTZSe, deposited by AGC method, have not been investigated either. The main objective in this study is to determine highest photoactivity from each source material ($S_M$ = TSe, CTSe, CTZSe) under different substrate temperature ($T_S$), argon gas flow rate ($V_A$) and annealing temperature ($T_A$), and study their effect on PEC characteristics. Correlation between electrode PEC characteristics and structural, morphological, compositional and optical properties has been investigated.

## 2. EXPERIMENTAL SECTION

### 2.1 Chemicals

Pottasium hexacyanoferrate (III), $K_3$ [Fe(CN)$_6$] and pottasium hexacyanoferrate(II) trihydrate, $K_4$[(Fe(CN)$_6$)].$H_2O$ were purchased from Sigma Aldrich. Hydrochloric acid, HCl was purchased from Friendmann Schmidt Chemical. Organic solvents, methanol and 2-propanol, were purchased from Merck KGaA and HmbG Chemicals respectively. Starting materials copper, tin, and selenium were all purchased from Alfa Aesar with nominal purity of 99.8, 99.5 and 99.5% respectively. Zinc was purchased from Nanostructured & Amorphous Materials Inc with nominal purity 99.9%.

*2.2 Film electrode preparation*

The TSe, CTSe and CTZSe alloy source materials were prepared using the melt-quenching method [36]. The polycrystalline TSe, CTSe and CTZSe compounds were synthesized from their constituent elements, which were weighed in stoichiometric 1:1, 2:1:3 and 2:1:1:4 nominal molar ratios, mixed, sealed in a quartz ampoule at base pressure of 0.33 Pa and heated. Each compound was taken out of the ampoule and ground into fine powder for XRD analysis. The XRD patterns were measured on an XPERT-PRO X-ray diffractometer with Cu $K_\alpha$ [1.54056 Å]. After confirming its structure by XRD, each prepared compound was then used as source material.

Thermal vacuum deposition procedure was typically conducted as follows: Each source material (0.10 g) was placed in a molybdenum evaporation boat. To obtain strong adherence and film uniformity, substrates of highly conductive ITO/glass slides was pre-cleaned prior to deposition. The substrate was mounted on a mask that was placed 14 cm above the boat. The set was then covered with a bell jar and evacuated to a vacuum of 5 X $10^{-4}$ Pa. A heater was kept directly above the substrate and set at desired temperature ($T_S$ = RT, 100, 200 or 300 °C) for every deposition. A thermocouple was used to monitor the substrate temperature.

Argon gas was introduced into the vacuum chamber via an inlet tube having a nozzle 0.5 mm in diameter at different flow rates ($V_A$= 5, 10, 15 or 25 cm$^3$/min). The nozzle was mounted near the evaporation boat, and its outlet direction was pointed towards the substrate. By gradually increasing the applied current, the source material powder melted, evaporated from the boat and deposited on the substrate. The as-deposited films were heated to desired temperature ($T_A$ = 150, 250, 350 and 450 °C) for 30 minutes under nitrogen gas atmosphere at ramp-up and ramp-down rates 5 °C/min.

Film thickness values for different films were measured using an Ambios-Tech XP-200 high surface profilometer. The atomic compositions of the films were investigated by EDX (Oxford Instruments model 7353) attached to a Nova NanoSEM 230 field emission scanning electron microscope (FESEM) to observe surface morphology. PEC experiments were performed using $[Fe(CN)_6]^{-3}/[Fe(CN)_6]^{-4}$ redox system, by running linear sweep voltammetry between +1.0 V and -1.0 V with a scan speed of 20 mV/s using a PGSTAT 101 Potentiostat. A conventional three-electrode cell, equipped with a platinum counter electrode and an Ag/AgCl reference electrode, was used. An Osram halogen lamp was used as a light source. The light intensity at the working electrode was measured to be 0.1 W/cm$^2$ by a pyranometer (LI-200; Li-Cor, USA) and used to directly illuminate the sample. The light was intermittently chopped up and down by a thick black cardboard at 0.5 cycles per second to give the effect of photocurrent and dark current.

## 3. RESULTS AND DISCUSSION

*3.1 Determination of highest photoactivity*

Figures 1a-c show PEC photoresponse values with chopped light illumination under linearly increased bias for films that exhibited highest photoactivity from each source material. Current

changed (increase/decrease) when the illumination was chopped (on and off) under cathodic bias (from 0 to -1 V vs Ag/AgCl) and under anodic bias (from 0 to +1 V vs Ag/AgCl). Carriers are presumably excited in the illumination region within the thin film and the excited minority carriers diffuse to the surface during their lifetime to participate in an electrochemical reaction at the film/electrolyte interface. The fact that the film electrodes exhibited both negative and positive photocurrents indicates that the films involved both n- ad p-type behaviors readily. The term p%, shown in Tables 1a and 1b, is the measured photoactivity calculated from the experimental value of photo current density ($J_P$) and dark current density ($J_D$) using the formula p% = [($J_P - J_D$)/$J_D$] x 100%. Photo and dark current density values at − 0.5 V for all samples were used to represent electrode photoactivity. Sample deposition conditions for as-deposited and annealed films, together with their effects on compositional and structural characteristics corresponding to photoactivity results, are summarized in Tables 1a and 1b.

The highest photoactivity, for TSe source-based films, was observed from the film deposited at $T_S$ = 100 °C under $V_A$ = 5 cm$^3$/min condition. The film deposited at 100 °C, which exhibited lower Sn/Se ratio, showed highest observed photoresponse values. The results suggest that selenium was a major factor that increased the photoresponse for the film deposited at 100 °C. Selenium is a well-known photosensitive material [37]. Annealing the as-deposited films further lowered photoresponse. The loss of Se, by annealing, is responsible for photosensitivity lowering.

The highest photoactivity for CTSe source-based films, was observed from the film deposited at $T_S$ = 200 °C under $V_A$ = 5 cm$^3$/min condition. The films deposited at 100 °C and 200 °C involved mixed phases of SnSe and SnSe$_2$. The films deposited at RT and 300 °C involved mixed phases of Cu$_{1.8}$Se and SnSe, and Cu$_2$SnSe$_3$ and SnSe respectively. They showed the lowest photoresponse among the series. However, under higher argon gas flow rate ($V_A$ = 25 cm$^3$/min) the deposited film exhibited higher photoresponse due to SnSe being a dominant compound in the film. Films with single phase compound are responsible for higher photosensitivity. Annealing at temperatures between 150 - 350 °C could improved crystallinity of the film but lead to the formation of porosities between adjacent grains and caused incompact surface coverage. Annealing at higher temperature 450 °C enhanced crystallinity but leads to the formation of mixed phases involving Cu$_2$Se and SnO$_2$. Porosity and mixed phases with Cu$_2$Se and SnO$_2$ presumably increased film internal resistance and resulted in poor charge transfer across the solid/redox couple interface. As a result, poor photoresponse was observed for annealed films.

In case of the CTZSe source-based films the highest photoactivity was achieved from electrodes deposited at $T_S$ = 100 °C under $V_A$ = 25 cm$^3$/min. Increasing the substrate temperature did not improve the film crystallinity, and lead to formation of other phases such as CZTSe, ZnSe, Cu$_{1.8}$Se and Cu$_2$SnSe$_3$. Together with the presence of amorphous phases, the mixed phases are the main factor that caused poor photoreponse. Films prepared under lower argon gas flow rates involved mixed compounds of CZTSe and ZnSe. Films prepared under higher flow rates were found to have a single phase SnSe with higher crystallinity. Annealing the film improved crystallinity but lead to the formation of mixed phases involving Cu$_2$ZnSnSe$_4$ and ZnSe (with mixed hexagonal and cubic structures) compound. Films with highly crystalline single phase compound are responsible for higher photosensitivity.

Figure 1a shows that the film electrodes deposited from TSe source material exhibit higher positive dark current at voltages more positive than +0.5 V, and higher negative dark current and negative photo current with photoactivity 8.3% at voltages more negative than -0.2 V. The fact, that photo current occurred at voltages more negative than -0.2 V, indicates p-type behavior and justifies the presence of SnSe compound, since it is p-type semiconductor [38]. The higher positive and negative dark currents might be due to poor film surface coverage on the substrate which causes dark current leakage. The positive dark current was lower at voltages more positive than +0.8 V and more negative than - 0.1 V respectively for film deposited from CTSe source material (Figure 1b). Photo current exhibited at voltages more positive than +0.8 V and more negative than -0.1V, indicates n- and p-type behaviors. It justifies the presence of SnSe and $SnSe_2$ compounds as SnSe and $SnSe_2$ are p-type and n-type respectively [38]. Due to improvement in dark current, photoactivity 34.8 % has been achieved. There was only slight lowering in dark current at voltages more positive than + 0.8 V for film deposited from CTZSe with photoactivity 55.7 % (Figure 1c). The fact, that photo current occurred at voltages more negative than -0.2 V, indicates p-type behavior and justifies the presence of p-type SnSe compound. Higher photoactivity obtained from CTZSe source film at $T_S$ = 100°C and under $V_A$ = 25 $cm^3$/min might be due to the improved surface coverage with highly crystalline single phase SnSe.

**Table 1a.** Sample preparation conditions, photoactivity (at - 0.5 V), and EDX and XRD results observed for as-deposited films

| Source material ($S_M$) | Condition ($T_S$, $V_A$) | p% | $\lvert J_P-J_D \rvert$ mA | $\lvert J_D \rvert$ mA | Notes |
|---|---|---|---|---|---|
| | | **As-deposited** | | | |
| Tse | (RT, 5) | 1.1% | 0.002 | 0.168 | Single phase SnSe; Sn/Se = 0.74 |
| | (100, 5) | **8.3%** | 0.102 | 1.230 | Single phase SnSe; Sn/Se = 0.72 Higher selenium responsible for higher p% |
| | (200, 5) | 3.9% | 0.014 | 0.360 | Single phase SnSe; Sn/Se = 0.73 |
| | (300, 5) | 1.0% | 0.014 | 1.468 | Single phase SnSe; Sn/Se = 0.78 |
| | (100,10) | 3.3% | 0.038 | 1.135 | Single phase SnSe; Sn/Se = 0.73 |
| | (100, 15) | 1.3% | 0.022 | 1.668 | Single phase SnSe; Sn/Se = 0.78 |
| | (100, 25) | 1.8% | 0.030 | 1.665 | Single phase SnSe; Sn/Se = 0.76 |
| CTSe | (RT, 5) | 1.3% | 0.052 | 4.029 | Mixed phases : $Cu_{1.8}$Se and SnSe |
| | (100, 5) | 2.9% | 0.045 | 1.531 | Mixed phases : SnSe and $SnSe_2$ |
| | (200, 5) | **34.8%** | 0.024 | 0.068 | Mixed phases : SnSe and $SnSe_2$ |
| | (300, 5) | 0.5% | 0.011 | 2.421 | Mixed phases : $Cu_2SnSe_3$ and SnSe |
| | (300,10) | 0.9% | 0.030 | 3.330 | Mixed phases : $Cu_2SnSe_3$ and SnSe |
| | (300, 15) | 0.4% | 0.016 | 4.564 | Mixed phases : $Cu_2SnSe_3$ and SnSe |
| | (300, 25) | 9.1% | 0.042 | 0.468 | Single phase : SnSe |
| CTZSe | (RT, 5) | 0.6% | 0.026 | 4.345 | Amorphous structure |
| | (100, 5) | 1.4% | 0.055 | 4.030 | Mixed phases : ZnSe and CZTSe |
| | (200, 5) | 0.6% | 0.026 | 4.170 | Mixed phases : ZnSe, CZTSe and $Cu_{1.8}$Se |
| | (300, 5) | 0.6% | 0.026 | 4.535 | Mixed phases : ZnSe, CZTSe, $Cu_2SnSe_3$ |
| | (100,10) | 23.6% | 0.401 | 1.702 | Mixed phases : ZnSe and CZTSe (higher crystallinity) |
| | (100, 15) | 45.9% | 0.152 | 0.331 | Single phase : SnSe |
| | (100, 25) | **55.7%** | 0.152 | 0.273 | Single phase : SnSe Higher crystallinity |

**Table 1b.** Sample preparation conditions, photoactivity (at - 0.5 V), and EDX and XRD results observed for annealed films

| Source material ($S_M$) | Annealed | | | | Notes |
|---|---|---|---|---|---|
| | Condition ($T_s$, $V_A$, $T_A$) | p% | $|J_P-J_D|$ mA | $|J_D|$ mA | |
| TSe | (100, 5, 150) | 1.5% | 0.051 | 3.457 | Single phase SnSe; Sn/Se ratio = 0.73 (Loss of Se by annealing) |
| | (100, 5, 250) | 1.2% | 0.041 | 3.303 | Single phase SnSe; Sn/Se ratio = 0.73 (Loss of Se by annealing) |
| | (100, 5, 350) | 0.2% | 0.005 | 3.516 | Single phase SnSe; Sn/Se ratio = 0.79 (Loss of Se by annealing) |
| | (100, 5, 450) | 0.7% | 0.027 | 4.009 | Single phase SnSe; Sn/Se ratio = 0.82 (Loss of Se by annealing) |
| CTSe | (300, 5, 150) | 1.8% | 0.034 | 1.951 | Single phase $Cu_2SnSe_3$ but with formation of porosities |
| | (300, 5, 250) | 0.6% | 0.030 | 4.890 | Single phase $Cu_2SnSe_3$ but with formation of porosities |
| | (300, 5, 350) | 0.6% | 0.031 | 4.879 | Single phase $Cu_2SnSe_3$ but with formation of porosities |
| | (300, 5, 450) | 0.5% | 0.024 | 4.527 | Mixed phases: $Cu_2SnSe_3$, $Cu_2Se$ and $SnO_2$ with formation of porosities |
| CTZSe | (100, 5, 150) | 0.5% | 0.022 | 4.743 | Mixed phases : $Cu_2ZnSnSe_4$ , ZnSe (Cubic) and ZnSe (Hexagonal) |
| | (100, 5, 250) | 4.0% | 0.025 | 0.619 | Mixed phases : $Cu_2ZnSnSe_4$ , ZnSe (Cubic) and ZnSe (Hexagonal) |
| | (100, 5, 350) | 14.3% | 0.025 | 0.173 | Mixed phases : $Cu_2ZnSnSe_4$ , ZnSe (Cubic) and ZnSe (Hexagonal) with |
| | (100, 5, 450) | 13.3% | 0.050 | 0.372 | higher crystallinity |
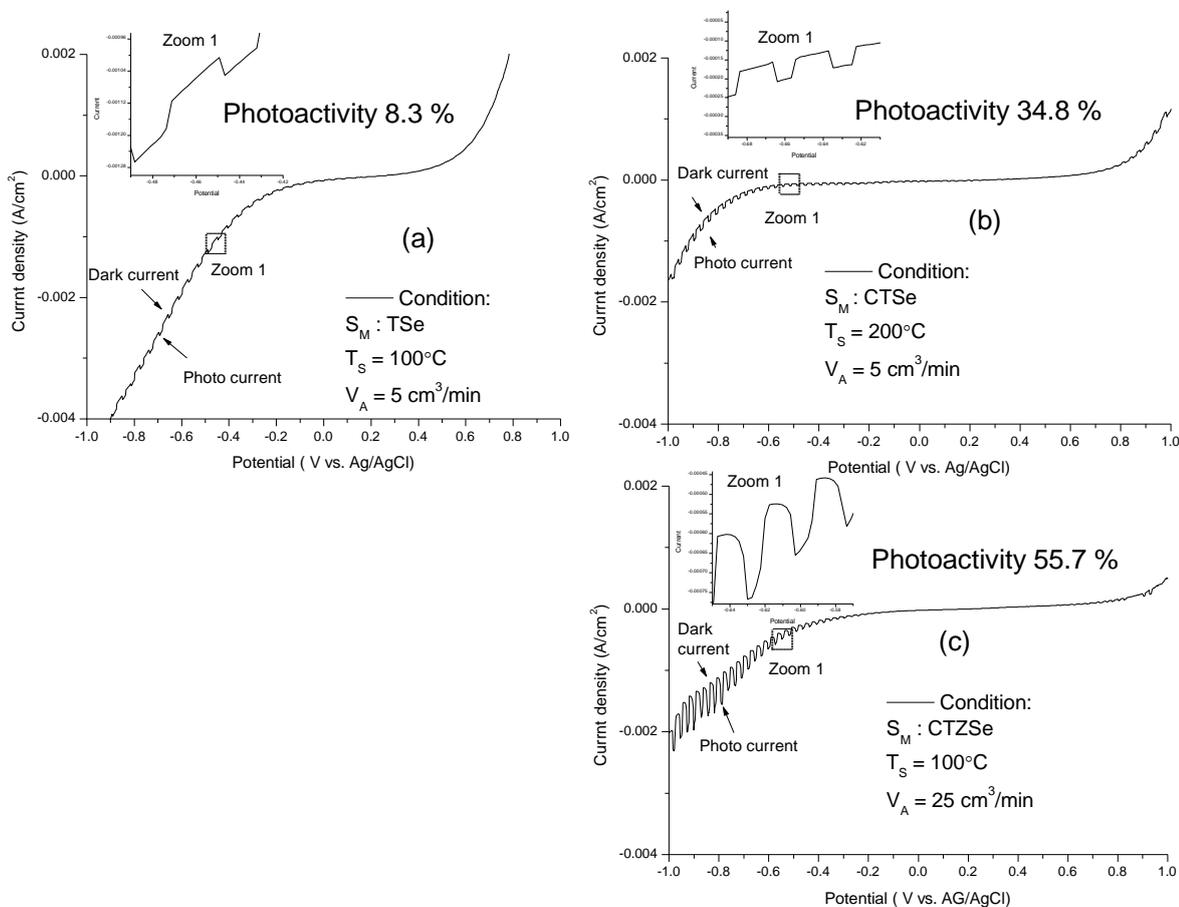


**Figure 1.** PEC characteristics measured for film electrodes deposited under different conditions

*3.2 X-ray diffraction*

The XRD patterns recorded for the deposited films with highest photoactivity from each source material are shown in Figures 2(d) - (f). The prominent Bragg reflection occurred at or around $2\theta = {\sim}30°$ corresponding to (111) for SnSe and (011) for $SnSe_2$ diffraction plane when compared with JPDS Card numbers 98-002-4334 (SnSe) and 98-004-8929 ($SnSe_2$) respectively. Combined together, the PEC characteristic results and the XRD patterns indicate that the deposited films presumably involved SnSe and $SnSe_2$. Figure 2(e) shows that the dominant peaks for SnSe (111) and $SnSe_2$ (011) planes overlap with the ITO/glass peak at or around $2\theta = {\sim}30°$. Film deposited from $S_M = TSe$ at $T_S = 100°$ under $V_A = 5$ $cm^3$/min involved highest crystallinity, followed by film deposited from $S_M = CTZSe$. Film deposited from $S_M = CTSe$ at $T_S = 200°$ under $V_A = 5$ $cm^3$/min exhibited poor crystallinity where a significant broad hump in the range $2\theta = 22° - 35°$ in the background indicates that the films involved amorphous phase.
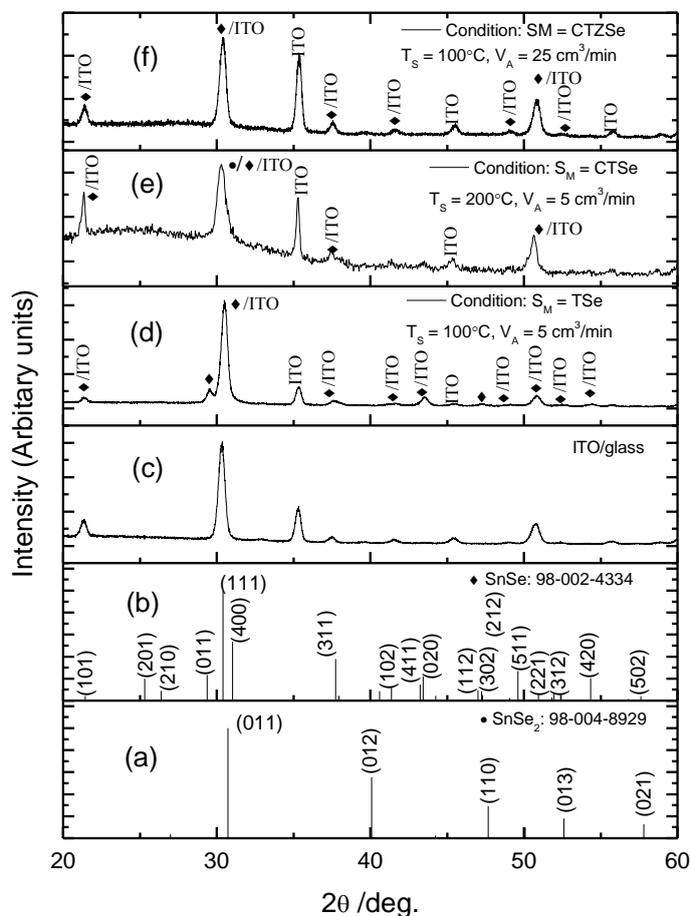


**Figure 2.** X-Ray diffraction spectra of a) SnSe, b) $SnSe_2$: JCPDS reference, c) ITO/glass, d) film deposited from TSe source at $T_S = 100$ °C under $V_A = 5$ $cm^3$/min, e) film deposited from CTSe source at $T_S = 200$ °C under $V_A = 5$ $cm^3$/min, and f) film deposited from CTZSe source under $T_S = 100$ °C and $V_A = 25$ $cm^3$/min

*3.3 Scanning electron microscopy*

Surface morphology, of films deposited from different source materials under various conditions, was investigated by SEM. Figure 3 shows SEM images for the film showing highest photoactivity deposited from each source materials. The SEM micrograph of the film deposited from $S_M$ = TSe at $T_S$ = 100° under $V_A$ = 5 cm$^3$/min, Figure 3(a), involved separate flaky particles with sharp edges. The film is incompact and does not fully cover the ITO/glass surface. The SEM micrograph of film deposited from $S_M$ = CTSe at $T_S$ = 200°C under $V_A$ = 5 cm$^3$/min, Figure 3(b), involved agglomerated small particles with higher compactness and film coverage. The SEM micrograph of the film deposited from $S_M$ = CTZSe at $T_S$ = 100° under $V_A$ = 25 cm$^3$/min, Figure 3(c), involved uniform round shaped particles with more compactness and full film coverage. Each film shows different surface morphology in parallel to its photoactivity performance. This shows that surface morphology significantly influenced PEC photoactivity.
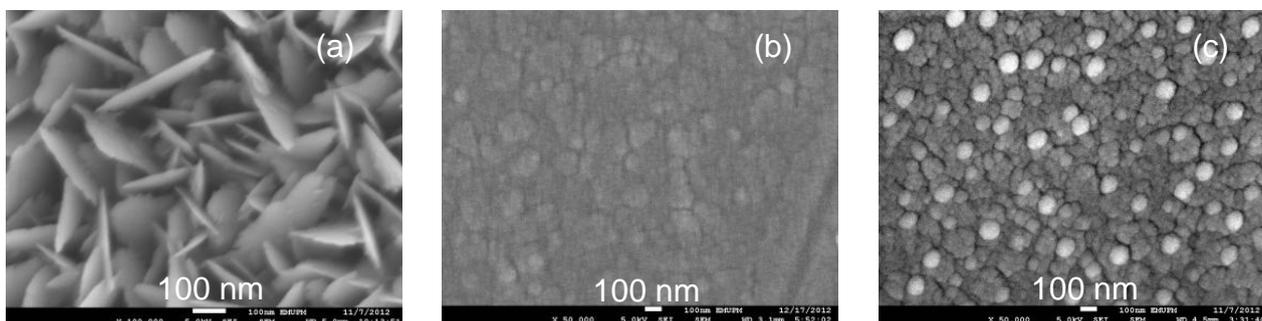


**Figure 3.** Surface morphology of films deposited under different deposition conditions a) film deposited from TSe source ($T_S$ = 100 °C and $V_A$ = 5 cm$^3$/min), b) film deposited from CTSe source ($T_S$ = 200 °C and $V_A$ = 5 cm$^3$/min), and c) film deposited from CTZSe source ($T_S$ = 100 °C and $V_A$ = 25 cm$^3$/min).

*3.4 Energy Dispersive X-Ray*

Energy dispersive X-Ray analysis (EDX) spectra were measured for each highest photo activity film deposited from each source material under various conditions. Five different points were measured on each film, each point having a scan area of 1 um x 1 um. The averaged atomic % values of each element together with standard deviations of the films are shown in Table 2. The three films showed homogenous compositions with only small standard deviations. The film deposited from $S_M$ = TSe ($T_S$ = 100° and $V_A$ = 5 cm$^3$/min) indicates an excess of selenium content. Films deposited from $S_M$ = CTSe ($T_S$ = 200° and $V_A$ = 5 cm$^3$/min) and from $S_M$ = CTZSe ($T_S$ = 100° and $V_A$ = 25 cm$^3$/min), exhibited significant differences in amounts of Sn and Se compared to Cu and Zn due to formation of SnSe/SnSe$_2$ and SnSe phases respectively. Smaller amount of Sn in films deposited from $S_M$ = CTSe and CTZSe and the loss of Cu and Zn, compared with film deposited from $S_M$ = TSe, indicates the

presence of free unreacted elements and/or amorphous phase. This result is consistent with XRD result.

**Table 2.** Values of average and Std. Dev. of atomic % for each element inside films deposited under different conditions.

| | Condition | Atomic % (Ave. of 5 points) | | | | Standard deviation (5 points) | | | |
|---|---|---|---|---|---|---|---|---|---|
| | | Cu | Zn | Sn | Se | Cu | Zn | Sn | Se |
| $S_M$ $T_S$ $V_A$ | Tse 100 °C 5 cm$^3$/min | n/a | n/a | 41.99 | 58.07 | n/a | n/a | 0.30 | 0.42 |
| $S_M$ $T_S$ $V_A$ | CTSe 200 °C 5 cm$^3$/min | 4.29 | n/a | 32.45 | 63.24 | 0.44 | n/a | 0.43 | 0.38 |
| $S_M$ $T_S$ $V_A$ | CTZSe 100 °C 25 cm$^3$/min | 4.50 | 9.56 | 24.18 | 61.77 | 0.96 | 0.65 | 1.05 | 1.14 |

Note: n/a = not applicable

*3.5 Optical Properties and Band Gap Energy*

Figure 4 shows absorption coefficient versus wavelength plots, obtained from UV-visible spectra, for the highest photo activity film deposited from different source materials under various conditions. The Figure shows relatively high absorption coefficient values ($> 10^4$ cm$^{-1}$) in the wavelength range 400 and 800 nm. This indicates that the films are active in the visible portion of the spectrum and could potentially be employed as visible light energy conversion materials. The film deposited from $S_M$ = CTZSe ($T_S$ = 100° and $V_A$ = 25 cm$^3$/min) shows higher absorption coefficient at waves shorter than 635 nm compared with the film deposited from $S_M$ = TSe ($T_S$ = 100° and $V_A$ = 5 cm$^3$/min). The film shows highest absorption coefficient at waves shorter than 475 nm when compared with film deposited from $S_M$ = CTSe ($T_S$ = 200° and $V_A$ = 5 cm$^3$/min). This explains why the film deposited from $S_M$ = CTZSe exhibited highest photoactivity as it absorbs more photons with higher absorption coefficient for the entire range of visible light. Sharp decrease in the area of wavelength more than 725 nm was observed for film deposited from $S_M$ = CTZSe, which indicates that unreacted metals are responsible for the amorphous nature and caused lower absorption. To determine the band gap energy ($E_g$) and the transition type of the semiconductor, the optical data were treated with the Stern equation by plotting the $(\alpha h v)^{2/n}$ versus $h v$, where $n=4$ for indirect transition materials and $n=1$ for direct transition [39]. The graphs, with extrapolation lines to the x-axis, are shown in Figures 5a - c. Estimated direct band gap value for film deposited from $S_M$ = TSe ($T_S$ = 100° and $V_A$ = 5 cm$^3$/min) was 1.28 eV, Figure 5b. The fact that this value is comparable with reported value for direct band gap

(1.21 eV) [40], indicates that the film involved SnSe compound. Ahn et al. [41] reported that films involving mixed copper zinc tin selenide and zinc selenide, should have band gap values in between their pure single phase band gap values. For SnSe films the reported $E_g$ value is 1.21 eV [40], and that for SnSe$_2$ films is 1.59 eV [38]. The direct band gap value for film deposited from $S_M$ = CTSe ($T_S$ = 200° and $V_A$ = 5 cm$^3$/min) was measured to be 1.45 eV, Figure 5c. The fact that the estimated direct band gap value is within the reported value range, indicates that the films involved a mixture of SnSe and SnSe$_2$. Estimated indirect band gap energy value for film deposited from $S_M$ = CTZSe ($T_S$ = 100° and $V_A$ = 25 cm$^3$/min) was 1.04 eV, Figure 5a. Literature shows that the SnSe film has an indirect band gap of 1.25 eV [42]. Thus the measured band gap value indicates that the film involved SnSe compound. Estimated direct band gap value for film deposited from $S_M$ = CTZSe ($T_S$ = 100° and $V_A$ = 25 cm$^3$/min) was 1.79 eV (Figure 5c) which is inconsistent with XRD result. A similar technique to identify the formation of SnSe compound, where XRD peaks overlap with ITO/glass peaks, has been reported earlier [43].
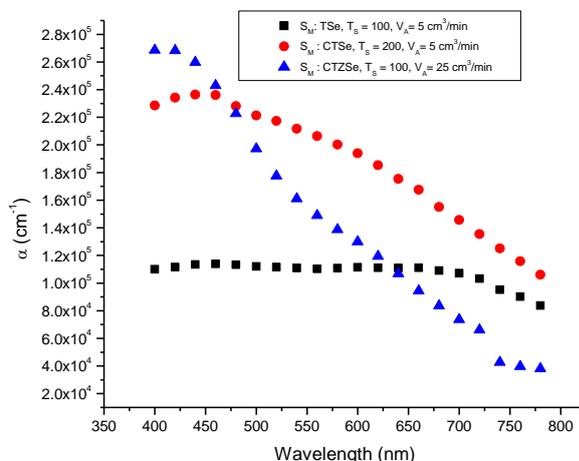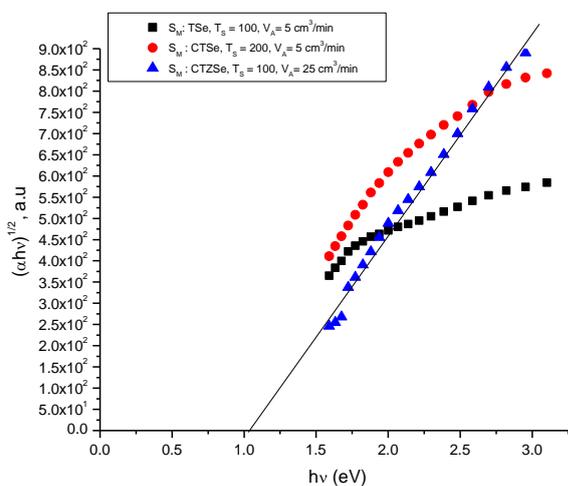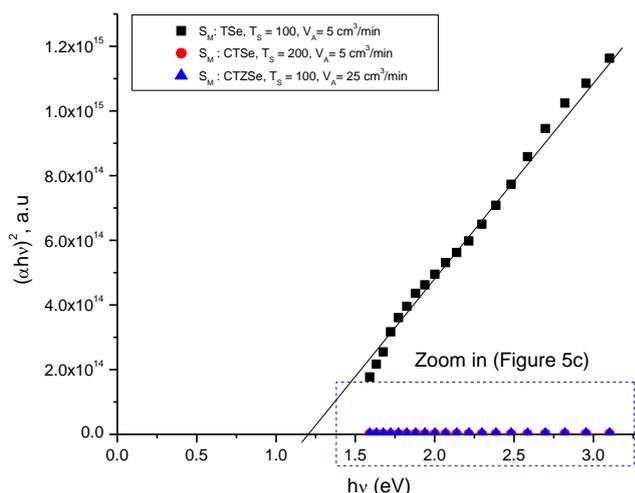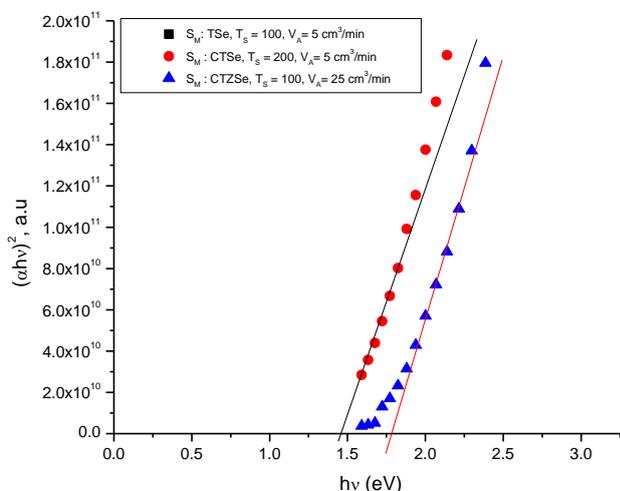


**Figure 4.** Absorption coefficient vs. wavelength plots for film deposited under different conditions



A

B



C

**Figure 5.** Plot of $(\alpha h\nu)^{2/n}$ vs. : (a) n = 4, (b) n = 1 and (c) n = 1 for samples electrodes deposited under different conditions

The combined results of XRD, EDX, photoresponses and optical properties of the films provide compelling evidence in favor of formation of SnSe or $SnSe/SnSe_2$ compounds by changing source materials under different substrate temperatures and argon gas flow rates. This highlights the potential of using quaternary CTZSe compound as source material to form SnSe film with lower dark current and higher photoactivity value under higher argon gas flow rate.


# 4. CONCLUSION

Film electrodes from different source materials under various substrate temperatures, argon gas flow rates and annealing temperatures, have been successfully deposited on ITO/glass substrate in

order to determine highest photoactivity from each source material. Among the different systems, the film with highest crystallinity but lowest photoactivity (p% = 8.3 %) was obtained from $S_M$ = TSe ($T_S$ = 100° and $V_A$ = 5 cm$^3$/min). The poor photoactivity was due to film surface morphology which involved flaky particles that were incompact with poor surface coverage. This electrode exhibited relatively high leakage dark current. The film deposited from $S_M$ = CTSe ($T_S$ = 200° and $V_A$ = 5 cm$^3$/min), exhibited more uniform film surface coverage on substrate with lowered leakage dark current. The amorphous phase that occurred in the film lowered its photoactivity (p% = 34.8 %). The film deposited from $S_M$ = CTZSe ($T_S$ = 100° and $V_A$ = 25 cm$^3$/min), exhibited highest photoactivity of p% = 55.7 % due to combination of better film surface coverage and higher compound crystallinity. It showed lowest dark current and highest photoresponse. The results manifest the added value of using a quaternary compound as a source material to deposit binary compound film electrodes in future processes while keeping eye to enhance PEC conversion efficiency.

**References**

1. M. Fujii, T. Kawai, S. Kawai, *J. Chem. Soc. Chem. Commun.*, (1985) 53-54
2. M. Fujii, T. Kawai, S. Kawai, *J. Electrochem. Soc.,* 136 (1989) 649-656
3. M. Fujii, T. Kawai, S. Kawai, *Sol. Energy Mater.*, 18 (1988) 23-35
4. C. B. Roy, D. K. Nandi, P. K. Mahapatra, *Electrochim. Acta*, 31 (1986) 1227-1229
5. R. K. Aloney, J. K. Dongre, B. P. Chandra, M. Ramrakhiani, *Chalcogen. Lett.*, 6 (2009) 569-575
6. A. A. Yadav, M. A. Barote, E. U. Masumdar, *Chalcogen. Lett.*, 6 (2009) 149-153
7. P. P. Hankare, P. A. Chate, D. J. Sathe, M. R. Asabe, B. V. Jadhav, *Solid State Sci.*, 10 (2008) 1970-1975
8. D. Wei, G. Amaratunga, *Int. J. Electrochem. Sci.*, 2 (2007) 897-912
9. R. K. Pandey, S. Mishra, Tiwari, P. Sahu, B. P. Chandra, *Sol. Energy Mater. Sol. Cells*, 60 (2000) 59-72
10. R. N. Noufi, P. A. Kohl, A. J. Bard, *J. Electrochem. Soc. Electrochem. Sci. Technol.*, 125 (1978) 375-379
11. T. Shikha, T Sanjay, *Sol. Energy Mater. Sol. Cells*, 90 (2006) 1621-1628
12. Z. Zainal, A. J. Ali, A. Kassim, M. Z. Hussein, *Malaysian Journal of Analytical* ,7 (2001) 197-202
13. N. Gagamarian, Z. Zainal, M. Zidan, W. T. Tan, *Int. J. Electrochem. Sci.*, 8 (2013) 312-322
14. J. Sharma, G. Singh, A. Thakur, G. S. S. Saini, N. Goyal, S. K. Tripathi, *J. Optoelectron. Adv. M.*, 7 (2005) 2085-2094
15. I. K. El-Zawawi, A. M. El-Shabiny, *Egypt J. Solids*, 27(2004) 223-232
16. P. S. Vincett, Z. D. Popovic, L. M. Intye, *Thin Solid Films*, 82 (1981) 357-376
17. S. M. Patel, N. G. Patel, *Mater. Lett.*, 2 (1983) 131-133
18. J. Sharma, S. K. Tripathi, *Phys.B*, 406 (2011) 1757-1762
19. N. Kumar, U. Parihar, R. Kumar, K. J. Patel, C. J. Panchal, N. Padha, *Am. J. Mater. Sci.*, 2 (2012) 41-45
20. M. A. S. M. Yunos, Z. A. Talib, W. M. M. Yunus, *J. Chem. Eng. Mater. Sci.*, 2 (2011) 103-109
21. P. A. Fernandes, P. M. P. Salome, A. F. Cunga, *J. Phys. D: Appl. Phys.*, 43 (2010) 1-11

22. G. Suresh Babu, Y. B. K. Kumar, Y. B. K. Reddy, V. S. Raja, *Mater. Chem. Phys.*, 96 (2006) 442-446
23. S. Hong, C. Kim, S. Park, I. Rhee, D. Kim, J. Kang, *Mol. Cryst. Liq. Cryst.*, 565 (2012) 147-152
24. G. S. Babu, Y. B. K. Kumar, P. U. Bhaskar, V. S. Raja, *Semicond. Sci. Technol.*, 23 (2008) 1-12
25. N. Kumar, V. Sharma, N. Padha, N. M. Shah, M. S. Desai, C. J. Pancal, I. Y. Protsenko, *Cryst. Res. Technol.*, 45 (2010) 53-58
26. K. J. John, B. Pradeep, E. Mathai, *J. Mater. Sci.*, 29 (1994) 1581-1583
27. R. Indirajith, T. P. Srinavasan, K. Ramamurthi, R. Gopalakrishnan, *Curr. Appl. Phys.*, 10 (2010) 1402-1406
28. A. Simchi, R. Ahmadi, S. M. S. Reihani, A. Mahdavi, *Mater. Des.*, 28 (2007) 850-856
29. C.C.Koch, *Nanostructured Materials:Processing, Properties and Applications*, second ed., William Andrew, Inc, Norwich, NY, 2007, 47-90
30. H. S. Hilal, R. M. A. Ismail, A. Hamouz, A. Zyoud, I. Saadeddin, *Electrochim. Acta*, 54 (2009) 3433-3440
31. Z. Zainal, S. Nagalingam, A. Kassim, M. Zobir. Hussein, W. M. M. Yunus, *Sol. Energy Mater. Sol. Cells*, 81 (2004) 261-268
32. K. Moriya, J. Watanabe, K. Tanaka, H. Uchiki, *Phys. Status Solidi*, 3 (2006) 2848-2852
33. S. Ahn, S. Jung, J. Gwak, A. Cho, K. Shin, K. Yoon, D. Park, H. Cheong, J. H. Yun, *Appl. Phys. Lett.*, 97 (2010) 0219051-02190513
34. B. G. SUrech, K. Y. B. Kishore, B. P. Uday, R. V. Sundara, *Sol. Energy Mater. Sol. Cells*, 94 (2010) 221-226
35. I. K. E. Zawawi, M. A. Mahdy, *J. Mater. Sci.: Mater. Electron.*, (2013)
36. N. Sabli, Z. A. Talib, W. M. M. Yunus, Z. Zainal, H. S. Hilal, M. Fujii, *Mater. Sci. Forum.*, 756 (2013) 273-280
37. K. S. V. Santhanam, M. Sharon, *Photoelectrochemical Solar Cells*, Elsevier Science, Inc, New York, NY, 1988, 156-177
38. D. M.Escobar, M. Ramachandra, A. S. Juarez, J. S. N. Rios, *Thin Solid Films*, 535 (2013) 390-393
39. F. Stern, *Solid State Physics* 15 (1963) 299-408
40. 41 K. J. John, B Pradeep, E. Mathai, *J. Mater. Sci.*, 29 (1994) 1581-1583
41. S. Ahn, S. Jung, J. Gwak, A. Cho, K. Shin, K. Yoon, D. Park, H. Cheong, J. H. Yun, *Appl. Phys. Lett.*, 97 (2010) 0219051-02190513
42. Z. Zainal, S. Nagalingam, A. Kassim, M. Z. Hussein, W. M. M. Yunus, *Mater. Sci.*, 21 (2003) 225-233
43. N. Sabli, Z. A. Talib, W. M. M. Yunus, Z. Zainal, H.S. Hilal, M. Fujii, *Int. J. Electrochem. Sci.*, 9 (2013) (in press).